Journal of Analytical and Applied Pyrolysis 169 (2023) 105841

Contents lists available at ScienceDirect

Journal of Analytical and Applied Pyrolysis

journal homepage: www.elsevier.com/locate/jaap

Production and characterization of bio-oil from fluidized bed pyrolysis of olive stones, pinewood, and torrefied feedstock

Anna Trubetskaya [a,*], Lukas von Berg [b], Robert Johnson [c], Sean Moore [d], JJ Leahy [e], Yinglei Han [f], Heiko Lange [g], Andres Anca-Couce [b,h]

[a] Department of Biosciences and Aquaculture, Nord University, Steinkjer 7715, Norway
[b] Institute of Thermal Engineering, Graz University of Technology, Inffeldgasse 25b, Graz 8010, Austria
[c] Arigna Fuels, Arigna Carrick-on-Shannon Co., Roscommon, Ireland
[d] Faculty of Science and Engineering, University of Limerick, Limerick, Ireland
[e] Department of Chemical Sciences, University of Limerick, Limerick, Ireland
[f] Department of Biological Systems Engineering, Washington State University, Pullman, WA 99164, USA
[g] Department of Earth and Environmental Sciences, University of Milano-Bicocca, Piazza della Scienza 1, 20126 Milan, Italy
[h] Carlos III University of Madrid, Thermal and Fluids Engineering Department, Avda. de la Universidad 30, 28911 Leganés, Madrid, Spain

ARTICLE INFO

Keywords:
Olive stones
Torrefaction
Bio-oil
Catalyst
Fuel feeding

ABSTRACT

Advancements in fluidized bed pyrolysis mechanisms and analytical methodologies are critical for progress in the biorefinery sector in general and the aviation fuel sector in particular. The statistical modelling of pyrolysis product yields and composition allowed us to observe advantages of operating temperature and feedstock selections over the torrefaction process and catalyst addition in a fluidized bed reactor. Results suggest that the chemical composition and physical properties of bio-oil from pyrolysis of olive stones at 600°C and pinewood pellets at 500°C are the most suitable for use as fuels. This work suggests that only combined use of selected gas chromatography mass spectroscopy, UV fluorescence, nuclear magnetic resonance spectroscopy, and rheology can provide comprehensive information on pyrolysis bio-oil composition. Importantly from a technological point of view, bio-oil was characterized i) by a viscosity similar to that of fossil-based oil; ii) by a low oxygen and water content; and iii) by a balanced composition of aliphatic and aromatic species. These factors indicate that bio-oil from fluidized bed pyrolysis of biomasses is a promising material for use in the aviation industry and energy production.

1. Introduction

Global consumption of non-renewable materials such as fossil fuels and minerals is expected to double in the next thirty years, while annual waste production is estimated to increase by approximately 70% by 2050 [1]. To keep resource consumption within planetary boundaries, it is necessary to minimize carbon emissions, lower collective and environmental footprint, and concurrently reuse / recycle the amount of current waste materials in the coming decades. Preventing food waste from being generated in the first place, and reducing its quantity in other cases, could have a major impact on waste collection systems and on the capacity of bio-waste management facilities worldwide [2]. Therefore, sustainable food waste management is a key aspect of sustainable economies and societies; one possibility for such a waste management in the context of a sustainable business strategy is to convert inevitable food waste into green fuels.

Biomass and food waste can be transformed into a liquid green fuel starting with pyrolysis processes. Fluidized bed reactors are being industrially used for combustion [3], gasification [4], and both non-catalytic [5] and catalytic pyrolysis [6]. Torrefaction is a mild pyrolysis process that converts biomass into a higher carbon material with increased energy density and concurrently reducing the water content [7]. The inhomogeneity of various molecular fractions in bio-oil can cause large problems during high-temperature biomass pyrolysis. Several attempts have been made to improve homogenity of bio-oil using various operating conditions and co-pyrolysis of several feedstocks in a fluidized bed reactor [8,9]. However, other literature sources report that torrefaction was able to improve the liquid homogeneity of

* Corresponding author.
E-mail address: anna.trubetskaya@nord.no (A. Trubetskaya).

https://doi.org/10.1016/j.jaap.2022.105841
Received 3 September 2022; Received in revised form 30 November 2022; Accepted 19 December 2022
Available online 23 December 2022

bio-oil [10,11]. The main components of condensable products from torrefaction are acidic products [12]. This suggests that the bio-oil from pyrolysis of torrefied biomass will contain less phenolics and carboxylic acids than that of non-treated feedstock [13,14]. In addition, the evolution of acetic acid during biomass torrefaction leading to a lower production of "phenolics" during pyrolysis is not well understood. Torrefaction pre-treatment did not improve yields of pyrolysis bio-oils, but rather formed greater yields of char [15]. The combination of torrefaction pre-treatment with the addition of CO_2 during pyrolysis of food waste in a bubbling fluidized bed reactor led to higher bio-oil yield, whereas the replacement of CO_2 with N_2 decreased the bio-oil yield, concurrently increasing the quality of a bio-oil with higher aliphatic and phenol contents [16]. Addition of zeolites into the fluidized bed reactor decreased the residence time and temperature, enabling conversion towards value-added products in a liquid phase [17]. Catalytic pyrolysis using HZSM-5 can increase aromatic hydrocarbon yields [18]. However, torrefaction process parameters must be properly adjusted to find the optimum torrefaction conditions for matching the subsequent catalytic pyrolysis. Previous fluidized bed pyrolysis studies have used torrefied pinewood, olive stones, wood chips and switchgrass [15,18–21]. To the authors' knowledge, not many studies have been conducted on fluidized bed pyrolysis of torrefied waste feedstock. Moreover, there is a lack of studies in which product yields and qualitative properties of produced bio-oil are combined to understand both the impact of the feedstock and the operating conditions. Several studies have emphasized the importance of feedstock origin on the bio-oil composition. The bio-oil sample obtained from pinewood pellets shows differences in composition that can be expected on the basis of the fundamental structural differences in terms of lignin-type. As a softwood sample, this bio-oil reflects the G-type lignin contained in the wood, e.g., lignin essentially constructed on the basis of coniferyl alcohol monomers. The olive stones comprise a GS-lignin, *i.e.*, a lignin made from both coniferyl and sinapyl alcohols as monomeric basis and displaying as such a rather different chemistry upon pyrolysis [22,23]. A recent study showed that only through utilizing a range of complementary analytical techniques information can be provided on light and heavy molecular tar fractions, allowing detection and characterisation of carbohydrates, phenolic and polyaromatic compounds [12]. However, High Resolution Fourier Transform Ion Cyclotron Resonance Mass Spectroscopy (FT-ICR MS) used to characterise tar or bio-oil structures with respect to molecular weight distribution and chemical formulas is difficult to apply in quantitative characterization analyses. This is due to the lack of detection for non-ionizable compounds during FT-ICR MS analysis, inhomogeneous nature of milled biomass particles, and limited global accessibility to the FT-ICR MS instruments [24]. A combined approach is required to determine the quantitative and qualitative properties of bio-oil to provide analysis simplicity and comprehensiveness.

In the present study, an approach for detailed compositional characterisation of pyrolysis bio-oil has been provided to establish a statistical model. The aim of this study was to evaluate the chemical composition of the bio-oil from fluidized bed pyrolysis of non-treated waste and torrefied material. ^{1}H NMR and GC-MS were conducted for bio-oil samples which were generated under different pyrolysis conditions to determine if there are any differences in their chemical composition. Viscosity of pyrolysis bio-oils was determined using a rheometer. Differences in physicochemical properties of pyrolysis bio-oil were correlated to operating conditions and feedstock type using a statistical model.

2. Materials and methods

2.1. Fluidized bed reactor

Pyrolysis tests of olive stones, torrefied olive stones and softwood pellets were conducted in a lab-scale fluidized bed reactor at 500 and 600°C. The obtained gas was fed to a condenser to capture heavy tars and water. Afterwards, part of the gas was sampled through impinger bottles to trap the remaining tars. Fig. 1 illustrates the flowchart of the experimental set-up.

The reactor was described in detail elsewhere [25]. The cylindrical bubbling fluidized bed reactor is made of stainless steel with an inner diameter of 80 mm and a height of 150 mm at the bed region. The inner diameter of 250 mm in the freeboard reduces gas velocity and prevents entrainment of bed material. The reactor is electrically heated and can achieve temperatures up to 900°C. Olivine was used as bed material and a mass flow of 1 kg h^{-1} N_2 ensured smooth fluidization of the bed. Biomass was fed from the hopper to the bed via a screw feeder. The turning rate was adapted to achieve the desired mass flow for different fuel types. A constant nitrogen flow of 0.05 kg h^{-1} was used to maintain an inert atmosphere in the fuel feeding system. In addition, the feeding rate was around 350 g h^{-1}. However, the feeding rate was measured for each experiment individually based on initial and remaining mass in the hopper to obtain accurate values. Gas released during pyrolysis was led through a hot filter to remove solid particles. Reactor pressure was maintained at 2 bar by a pressure regulator. The residence time in the bed was about 1 s, whereas it was about 15 s in the freeboard (for experiments at 600°C and 2 bar).

The condenser is realized as a heat exchanger tube bundle made of stainless steel. The outer housing has an inner diameter of 72 mm. The gas flow is lead through 16 inner tubes of 10 mm diameter (from top to bottom), whereas the cooling liquid is flowing from the bottom to the top (see Fig. 1). The total "active length" (where the gas going through the tubes shares a contact area with the cooling liquid) is 680 mm. A reservoir of about 0.6 litre at the bottom of the condenser collects the pyrolysis oil during the experiment. After leaving the reactor, the gas was led to a condenser were heavy tars and water are captured. All gas lines up to the condenser are electrically heated to 375°C to avoid condensation in the gas lines. The condenser temperature was set to a temperature of 35°C which was kept constant using a LAUDA thermostat. Heavy tars and water were captured in the condenser. Light tars and water still remaining in the gas phase after the condenser were captured using washing bottles. A setup similar to the tar protocol using 5 washing bottles at 35°C and − 20°C was employed with isopropanol as solvent. The bio-oil was separated into the light and heavy compound fractions using a centrifuge (Thermo Scientific Heraeus Biofuge Stratos, USA) at 7000 rpm and 10°C for 30 min

The flow rate of gas obtained after the condensation system was measured using a diaphragm gas meter. Finally, concentrations of O_2, CO, CO_2, CH_4, and H_2 were measured using an online permanent gas analyzer ABB AO2020. The difference to 100% was assumed to be N_2. Remaining gases, including the gas analysis outlet were burned in a flare. In comparison, the gas composition of samples was measured using a micro gas chromatography (micro-GC) instrument INFICON 3000 (Agilent Technologies, Ireland). The micro-GC was calibrated using a mixture of H_2, CH_4, N_2, CO, CO_2, C_2H_2, C_2H_4, C_2H_6, and H_2S. The O_2 content was calibrated using air.

For each test, the reactor was filled with 900 g olivine and the bed was heated to the operating temperature of 500 or 600°C while being flushed with N_2. Several experiments with ZSM-5 catalyst including 10% Ni were performed. As soon as constant temperature in the bed was achieved, biomass was fed to the reactor for about one hour. After about one hour, the biomass feeding was stopped. A mixture of bio-oil and water was extracted from the collection reservoir at the bottom of the condenser. Measuring the weight of the washing bottles filled with isopropanol before and after the test allowed calculation of the amount of tar and water trapped in the solvent. Three tests were conducted in a row. Afterwards, the fluidized bed reactor was opened to remove the produced char. Cleaning of the reactor was performed after each set of experiments to avoid fouling.

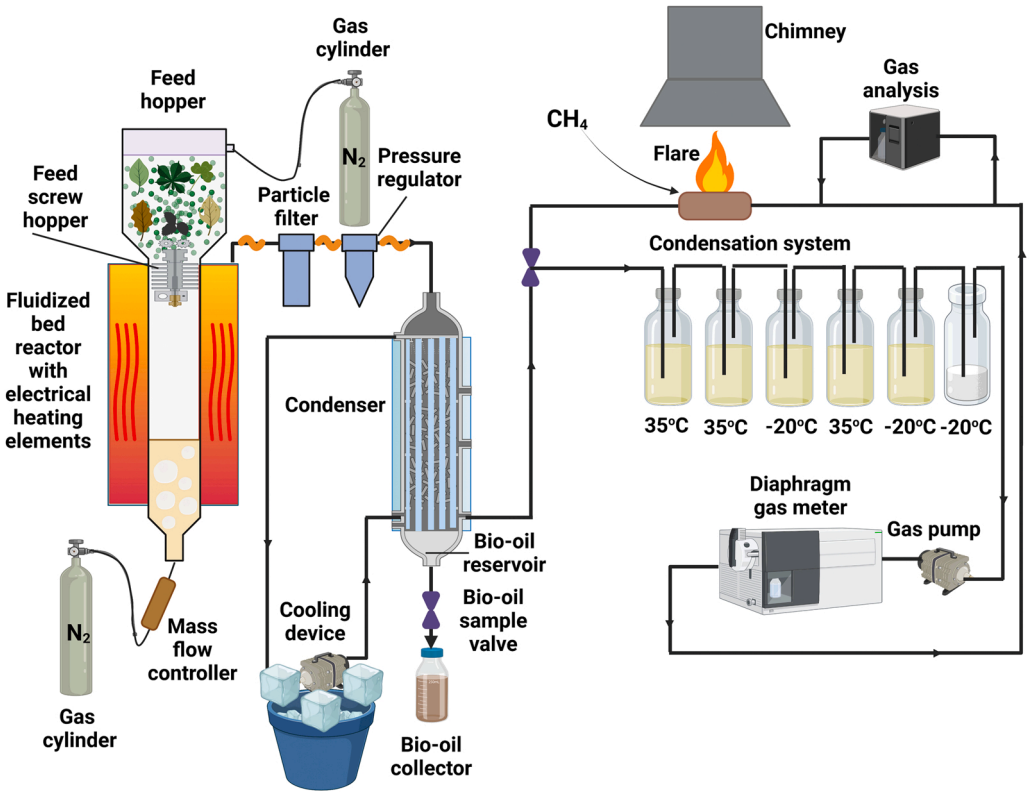

Figure 1. Flowchart of the experimental set-up.

2.2. Torrefaction

Olive stones from Tunisia were chosen as a feedstock based on their high bulk density and abundance. Particle size, bulk density and skeletal density of original olive stones were 0.8–5 mm, 0.6 g cm^{-3} and 1.5 g cm^{-3} respectively [26]. Olive stones were torrefied in a pilot-scale reactor at 280°C during a 24 h long production run [27]. The torrefied biomass is cooled to room temperature, further crushed and briquetted.

2.3. Characterization of pyrolysis products

2.3.1. Elemental analysis

Elemental analysis was performed on the instrument (Thermo Scientific Flash Smart, USA) that includes two combustion ovens, one for CHNS and the other for oxygen quantification. 2,5-Bis(5-*tert*-butyl-2-benzo-oxazol-2-yl) thiophene (BBOT) was used as a reference standard. The ash content was determined using a standard ash test at 550°C, according to the procedure described in DIN EN 14775. All measurements were conducted in duplicate to establish reproducibility. The experiments had an error of less than 2 %.

2.3.1.1. Karl Fischer titration. Karl Fischer titrations were conducted using a KF1000 volumetric titrator (Hach, Germany). Tar samples were first dissolved in anhydrous methanol and then injected into the titration cell. All titrations were conducted at room temperature and the experiments had an error of ± 0.5% water content.

2.3.1.2. Rheometer. Stored deformation energy (G′) of the heavy molecular bio-oil fraction was measured in pascals (Pa) using a Discovery Hybrid Rheometer-2 (TA Instruments, Ireland), as reported in previous studies [12].

2.3.1.3. Fluorescence UV analysis of bio-oil. The oils were diluted in HPLC-grade methanol at 20 ppm and analyzed using a Shimadzu RF 5301 pc (Panorama Fluorescence 2.1) spectrometer. Synchronous fluorescence spectra at a constant wavelength difference were set. The excitation wavelength was scanned from 235 to 700 nm, and emission wavelengths were recorded with 15 nm difference (from 250 to 715 nm). The excitation slit width and emission slit width were set at 3 nm. Data was collected every 1 nm. Samples at different concentration levels (1, 10, and 100 ppm) were evaluated and showed the same profile as with 100 ppm to rule out the self-absorption effect.

2.3.1.4. Gas Chromatography - Mass Spectrometry. The liquid products were analyzed by GC-MS using an Agilent Technologies 7890A GC coupled with the Agilent 5975 C mass spectrometer, using an Agilent column (19091S-433: 60 m x 250 μm x 0.25 μm). Aliquots for sample analyses were analysed in form of approximately 2 wt% blend with methanol (HPLC grade). As GC-MS analytical method was used: front inlet: 300°C, total flow He 24 mL min^{-1}, septum purge flow 3 mL min^{-1}; split ratio 7:1, 20 mL min^{-1}; column flow: 0.5 mL min^{-1}; and oven: 35°C for 3 min, ramp to 180°C at 2°C min^{-1}, ramp to 300°C at 20°C min^{-1}, and hold 3 min. NIST 2.0 Mass Spectral was used for peak identification.

2.3.1.5. Qualitative ^1H NMR analysis. Samples of around 15 mg were dissolved in 600 μl $CDCl_3$; ^1H NMR spectra were recorded at 27°C on a Bruker 400 MHz instrument equipped with TopSpin 2.1 software applying the Bruker zgpulse program in DQD acquisition mode, with NS = 64; D1 = 8 s. NMR data were processed with MestreNova; spectra were referenced to the residual signal of $CHCl_3$ in $CDCl_3$ (7.26 ppm).

2.3.1.6. Scanning electron microscopy. SEM imaging was performed using a Hitachi SU-70 scanning electron microscope at a gun voltage of 15 kV and using a secondary electron detector. Prior to imaging, pellet samples were crushed and loaded on a carbon tape and sputtered with 5 nm of gold.

2.3.1.7. Statistical analysis. Statistical modeling was performed using SAS JMP 15.0 (Frankfurt, Germany). Analysis of variance (ANOVA) was performed to evaluate the effect of operating conditions and feedstocks on the results of component analysis and product yield from pyrolysis in a fluidized bed reactor. Linear regression using scatterplot representation was performed to evaluate the relationship between operating conditions and bio-oil composition. All analyses were performed at significance level with $\alpha = 0.05$.

3. Results

3.1. Original feedstock characterization

Compositional analyses of olive stones after 6 months of storage at the Arigna Fuels' pilot plant and after further milling and sieving are shown in Table 1. As expected, torrefied olive stones have lower moisture and oxygen content, with corresponding higher carbon and higher heating values, when compared to wood pellets and raw olive stones [28].

The ash content of wood pellets is lower than that of olive stones. However, olive pits contained more potassium, silicon, and calcium than wood pellets [27]. Regarding mineral matter composition, the sodium content of wood pellets is exceptionally low compared to values of wood pellets from other studies [29,30]. Sodium is likely present as inorganic salts, with minor quantities associated with organic structures [31].

3.2. Impact of operating conditions on the product yields

In this study, 21 samples in total were collected from fluidized bed pyrolysis and a statistical analysis of product yields was conducted. Table 2 shows a summary of the most representative samples which were analyzed using elemental, and Karl Fischer analyses.

The composition of bio-oil and char will be discussed in sections below. Fig. 2 illustrates the product yields from 21 treatment combinations of olive stones (**OS**), torrefied olive stones (**TOS**) and pinewood pellets (**PP**) from pyrolysis using the SAS JMP Pro 15.2 statistical software. The graphical analysis shows the average response yields of bio-oil, solid char and gas as temperature, fuel type and catalyst addition are varied. The mean responses for each factor combination are indicated by the horizontal black line. The median and 25% and 75% quantiles are overlayed with a Box Plot in red. In all cases, the mass balance closure was > 80%. The results indicate that temperature is the dominant factor and is both practically and statistically significant. At 500°C, a bio-oil yield with an average of 42 wt% can be achieved with gas and char yield at 22.5 wt% and 22 wt% respectively. Once the temperature variable is changed to 600°C a negative correlation is observed with the bio-oil yield dropping to 33 wt%, alongside an increase in gas yield from 22.5 to 35 wt%. Char yields from pyrolysis of all feedstocks remained approximately stable at 21 wt% which is despite visual evidences from the box plot analysis indicating that variation increases with temperature settings of 500°C. This could be related to a more homogeneous feeding of pinewood pellets in a fluidized bed reactor due to smooth pelletized surface compared to the other feedstocks. Overall, the pyrolysis of pinewood pellets at 500°C led to lower char yield than pyrolysis of non-treated and torrefied olive stones, whereas gas and bio-oil yields were in an acceptable range.

Several experiments were performed with the 10% Ni doped ZSM-5-catalyst due to its proven potential to catalyze reactions leading to a decomposition of higher molecular weight compounds in the gaseous bio-oil phase, as well as deoxygenation reactions of compounds in the gas phase, as previously reported [32]. The two reaction types, *i.e.*, decomposition and deoxygenation, that are catalysed by the zeolite explain the slightly higher char yields observed in the presence of the catalyst during fluidized bed pyrolysis.

Previous studies have reported product yields from fluidized bed pyrolysis using corn straw as a feedstock in the temperature range from 450 to 550°C which are consistent with the yields in this study [33]. The main difference was observed for char and gas yields which were at about 40 wt% and 10 wt%, whereas the current study char and gas yields varied from 17.5 to 24 wt% and from 15 to 26 wt% in 500°C pyrolysis. This can be explained by the higher ash content in corn straw and consequently greater fraction of alkali metals which could lead to higher char yields during corn straw pyrolysis [34,35].

3.3. Catalyst characterization

The characterization of the virgin catalyst has been previously reported [32]. In order to analyse how the catalyst is affected by the pyrolysis process, the ZSM-5 catalyst pellet was separated from olivine and

Table 1
Proximate, ultimate and ash compositional analysis.

	Pinewood pellets	Olive stones	Torrefied olive stones
Proximate analysis			
Moisture, (wt% ar)	6.9	15.5	2.5
Ash at 550°C/815°C, (wt% db)	0.4	0.8	0.5
Volatiles, (wt% db)	80.8	75.5	75.1
HHV, (MJ kg^{-1} ar)	19.2	19.5	19.6
LHV, (MJ kg^{-1} ar)	17.7	18.0	18.2
Ultimate analysis, (wt%, dry basis)			
C	48.7	47.2	51.9
H	2.2	6.1	6.1
N	0.2	0.1	0.1
O	48.5	46.2	41.5
S	0.01	0.02	0.02
Cl	0.01	0.02	0.02
Ash compositional analysis, (mg kg^{-1}, dry basis)			
Al	15	40	10
Ca	1000	1900	700
Fe	60	40	30
K	600	3200	2300
Mg	120	80	50
Na	40	70	40
P	70	50	40
Si	1100	350	350
Ti	3	2	2

Table 2
Summary of collected samples (olive stones: OS; torrefied olive stones: TOS; pinewood pellets: PP) after pyrolysis in a fluidized bed reactor at 500 and 600°C with and without a catalyst and further analyzed in this study.

Feedstock	OS	TOS	TOS	PP	OS
Temperature /°C	500	500	500	500	600
Catalyst presence	no	no	yes	no	no
Bio-oil characteristics					
C, %	74.4 ± 0.1	71.6 ± 0.3	72 ± 0.15	71.6 ± 0.2	77.7 ± 0.1
H, %	6.3 ± 0.2	6.2 ± 0.2	6.2 ± 0.1	6.3 ± 0.4	6.2 ± 0.25
N, %	1.1 ± 0.05	0.8 ± 0.2	0.7 ± 0.3	0.3 ± 0.2	1.7 ± 0.1
O, %	18.2 ± 0.5	21.1 ± 0.2	21.1 ± 0.4	21.8 ± 0.4	14.4 ± 0.2
Water, wt%	8.9 ± 0.1	13.1 ± 0.5	18.8 ± 1.5	16.9 ± 0.9	10.4 ± 1.1
Ash, wt%	0.05 ± 0.01	0.06 ± 0.02	0.05 ± 0.02	0.02 ± 0.01	0.05 ± 0.02
Char characteristics					
Water, wt%	3.6 ± 0.2	2.3 ± 0.2	2.6 ± 0.2	1.9 ± 0.1	3.6 ± 0.2
Ash, wt%	5.9 ± 0.1	5.1 ± 0.1	5.6 ± 0.2	2.4 ± 0.2	6.6 ± 0.2

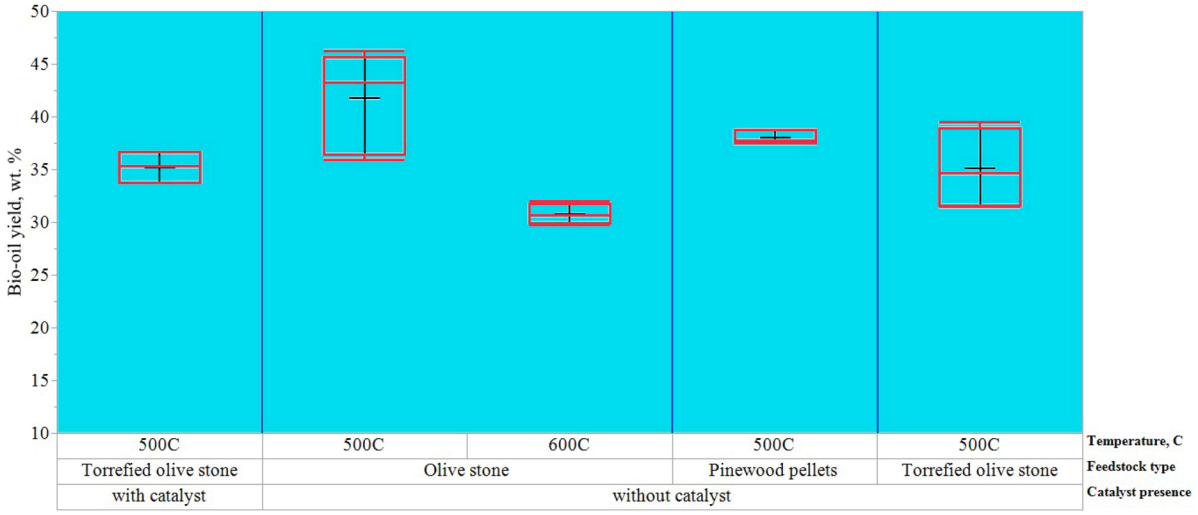

(a): Bio-oil distribution

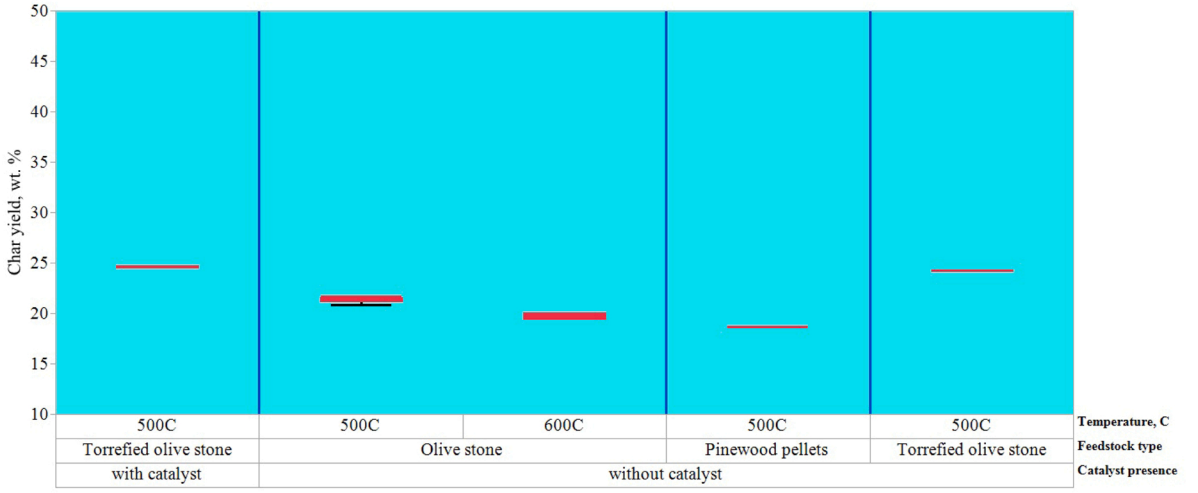

(b): Char distribution

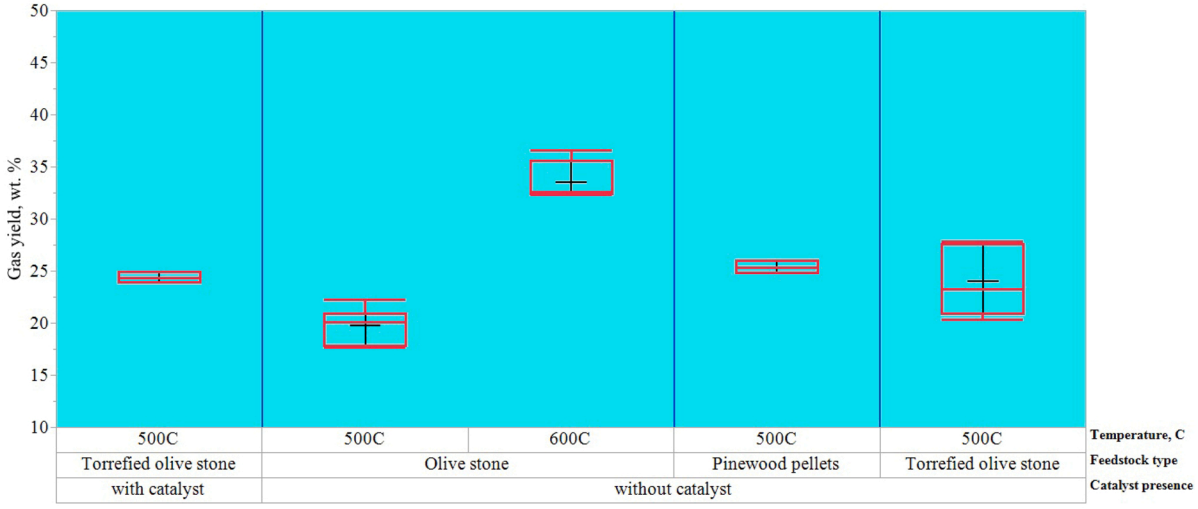

(c): Gas distribution

Figure 2. Variability charts of bio-oil, char and gas yields of 21 samples.

reacted char using sieving and further analyzed using BET analysis and SEM imaging. The specific surface area measurements of ZSM-5 after fluidized bed pyrolysis using N_2 adsorption are shown in Fig. 3.

The N_2 adsorption isotherm of catalyst shows the co-presence of micropores and mesopores. The features of the isotherms indicate fillings of both micropores and primary mesopores. The isotherm plot shows high nitrogen uptake at low relative pressure in the relative pressure p/p_0 range 0 and 0.4, typical for microporous materials [32]. Differences between adsorption and desorption isotherms are relatively small forming a hysteresis above a relative pressure p/p_0 of 0.4, as previously reported for H4 hysteresis loop [36]. However, this hysteresis indicates a presence of mesopores. The average surface area observed on the ZSM-5 catalyst was 165 $m^2\ g^{-1}$, whereas the cumulative pore volume varies from 0.04 to 0.27 $cm^3\ g^{-1}$. No significant changes were thus observed for the BET parameters of spent ZSM-5 catalyst.

The surface of the virgin ZSM-5 catalyst and cross section of the spent catalyst after pyrolysis are shown in Fig. 4. Fig. 4 (a) illustrates a high crystalline structure of virgin catalyst due to the presence of separated large segments which are connected by small particles. The small and large segments are more visible in the cross section of a catalyst after pyrolysis in a fluidized bed reactor. The catalyst structure remained similar to that of the non-treated pellet. Prior to SEM analysis, a ZSM-5 catalyst pellet was oxidized at 900°C for 12 h in the electrical furnace to remove the coke layer. Fig. 4(b) shows that coke formation during catalytic pyrolysis did not affect the morphology of a catalyst and thus, did not deactivate its properties. Moreover, the carbon layer removal from a catalyst surface indicates a regenerating potential of zeolites.

3.4. Gas composition

Figure 5 shows the main gases which were determined during fluidized bed pyrolysis using a gas analyzer and a micro-GC instrument. Concentrations of H_2, CO, CO_2, H_2S, CH_4, and C_xH_y (C_2H_2 and C_2H_4) during micro-GC analysis are shown for pyrolysis of olive stones (**OS**), torrefied material (**TOS**), and pinewood pellets (**PP**) at 500 or 600°C. The main difference of micro-GC analysis to the gas analysis with the ABB instrument is an additional detection of C_xH_y and H_2S gases. The micro-GC analysis identified higher concentrations of H_2 and CO_2 compared to the ABB gas analyzer, whereas concentrations of CO and CH_4 were found in a similar concentration range using both instruments. The continuous use of a micro-GC could support a precise closure of mass balances for all experiments.

The gas composition (CO_2, CO, CH_4, H_2) increased with increasing heat treatment from 500 to 600°C. The higher yield of CO_2 is due to intensified cracking of carboxyl functional groups at 600°C, whereas CO and H_2 yields could increase for several reasons [37], such as tar cracking, reforming of volatile matter, water gas reaction, or reverse Boudouard reaction [38]. The hydrocarbon cracking reactions could lead to increase of CH_4 concentration [39]. The catalytic pyrolysis of olive stones (**OS**) at 500°C and pyrolysis of pinewood pellets (**PP**) led to a decrease in CO_2 formation and increase in H_2 and CO fractions, as reported previously [40]. The increase in H_2 during catalytic pyrolysis could be due to hydrocarbon cracking compared to the torrefied olive stone (**TOS**) pyrolysis [41].

3.5. GCMS

The light fractions of bio-oil samples were analyzed using GCMS. Fig. 6 shows that for 5 representative samples of which acetic acid, 1-hydroxy-2-propanone, and phenol were most abundant with trace amounts of levoglucosan, propanoic acid, furfural, phenol and methoxyphenols. Levoglucosan that is known to indicate the partial cracking of carbohydrates was not in evidence in the tar samples of olive stones (**OS**) from pyrolysis at 500 and 600°C. Alkali metals are known to inhibit the formation of levoglucosan from cellulose and to favor formation of furfural from furans and carbonyl compounds like acetaldehyde and acetol from acids in pyrolysis [42,43]. Bio-oil from catalytic pyrolysis of torrefied olive stones (**TOS**) is richer in levoglucosan than bio-oil from **TOS** without catalyst use, despite the fact that similar furfural amounts were present in both samples. The catalyst enhanced the formation of levoglucosan in pyrolysis of **TOS**. Pyrolysis leads to the formation of larger levoglucosan-based oligomeric molecules capable of blocking catalyst pores and hindering the entrance of thermally cracked compounds into catalysts channels [44]. At later stages these molecules can undergo re-polymerization and condensation on the external catalyst surface by forming coke deposits [45]. Guaiacol and 2-methoxy-4-methyl substituted phenol are derived from the lignin fraction in olive stones and pinewood [46].

Phenolic compounds are derived from lignin by cracking the phenylpropane units and were detected in all bio-oil samples [47]. The fraction

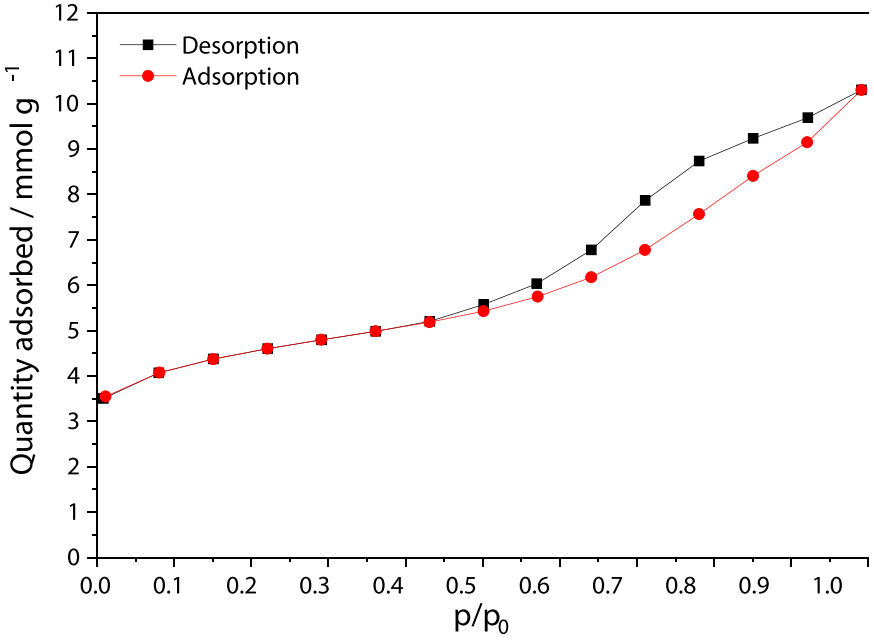

Figure 3. BET analysis of the catalyst pellet before and after use.

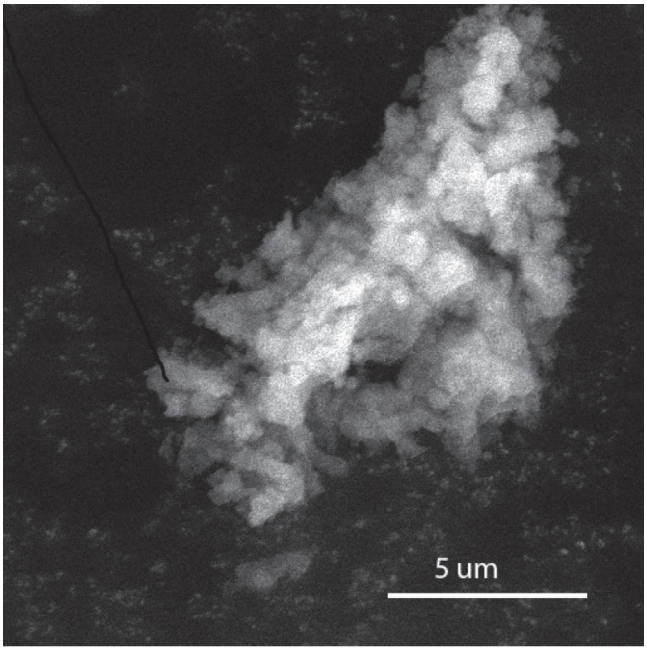

(a): Raw catalyst surface

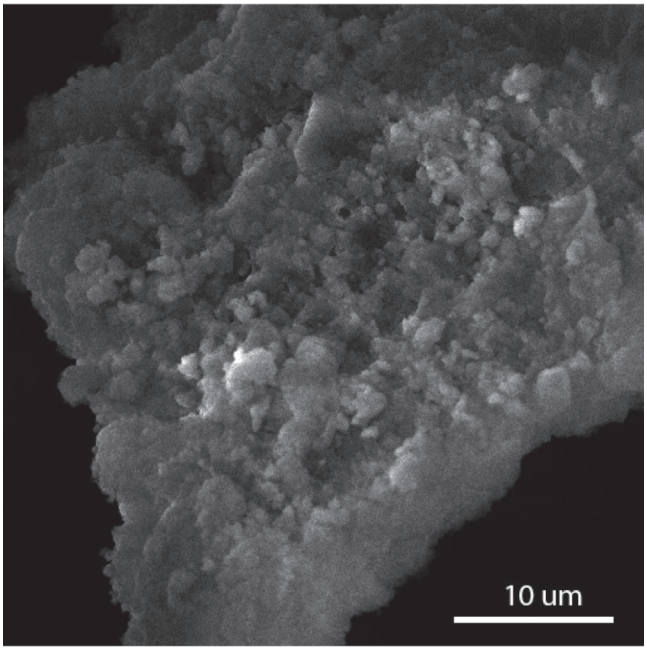

(b): Catalyst surface after pyrolysis

Figure 4. SEM imaging of ZSM-5 catalyst before and after pyrolysis in a fluidized bed reactor.

of lignin in torrefied samples can increase when hemicellulose fraction in lignocellulosic biomass decomposed [48].

In addition, a lower relative peak area of 1-hydroxy-2-propanone was detected in bio-oil from torrefied olive stones (**TOS**) compared to other samples due to the decomposition of small molecular mass compounds of hemicellulose and cellulose in torrefaction [49]. However, 1-hydroxy-2-propanone remains as one of most abundant compounds for all bio-oil samples. The main quantitative compositional difference was identified in acetic acid concentrations. Differences in the content and the chemical structure of hemicellulose are the main cause of differences in acetic acid yields. Table 3 illustrates that those differences in the relative areas of other compounds are lower in bio-oil from pinewood pellets (**PP**) than in samples from pyrolysis of olive stones (**OS**) corresponding to previous results [50]. Bio-oil samples from torrefied olive stones were enriched in phenolic compounds, independent of the use of a catalyst or not. Thus, **PP** bio-oil showed the lowest content of acetic acid due to the lower amount of hemicellulose compared to **OS**. It had been noted before that the acetyl content of softwood was about 1%, while that of hardwood and grasses varied between 3% and 6% [51, 52]. The acetyl content of olive stones and torrefied material was higher than that of pinewood, resulting in higher acid content in pyrolysis bio-oil.

The bio-oil samples were collected in gas wash bottles filled with isopropanol following a previously published protocol [53]. Isopropanol is the most effective homogenizer over butanol, ethanol, and propanol, since it keeps the oil in a single phase for the longest duration in the temperature range between − 20 and 80°C [54]. Methanol was found to be slightly less effective than isopropanol on the stability and aging properties of bio-oil [55]. Moreover, methanol is a more risky solvent for the environment and human health to use in pyrolysis experiments than isopropanol. Both isopropanol and methanol could intensify the formation of esters from carbolyxic acids [56]. However, the main advantage of both polar protic organic solvents is in the dissolution of essentially all compounds contained in the oil [57].

The previous tar analysis results were represented in terms of the following tar classes: GC-undetectable tars (class 1), heterocyclic compounds (class 2), aromatic compounds (class 3), light polyaromatic compounds (class 4), and heavy polyaromatic compounds (class 5) [58]. Soxhlet treatment aiming to separate bio-oil compounds from isopropanol or methanol could lead to a loss of most of class 3 components, fractions of class 4 and 2 components due to the low boiling point [59]. For the analysis of the various components, ^{1}H NMR and GCMS analyses can be eventually seen complementary in the chosen experimental design of this study.

3.6. ^{1}H NMR

NMR techniques are standard analysis tools for gaining insights into pyrolysis oil compositions [60]. In this work, ^{1}H NMR analysis was applied to the pyrolysis oils under study, as shown in Fig. 7. The light and heavy bio-oil fractions were separated prior to ^{1}H NMR analysis. As indicated in Fig. 7(a), some functional groups can generally be obtained, which by and large are in close correspondence to the results identified by GCMS. In order to account for eventually present issues in solubilities, samples were run in both deuterated chloroform (see Fig. 7(b)) and deuterated acetone (see Fig. 7(c)) as solvent.

Fractionation in light and heavy bio-oil fractions was done in the simplest mode possible, and thus traces of any of the contained functional motifs were seen in both fractions, independent of the solvent used for analysis. Generally, higher solubility was found in acetone, especially for the heavy fraction of the bio-oil from pyrolysis at 600°C. It can nevertheless be delineated that aldehydes and carboxylic acids are mainly found in the light fraction. Aromatics and unsaturation motifs are, on the contrary, clearly enriched in the heavier, viscous fraction. Due to the fact that the oil was taken up in isopropanol, some functionalities and can only roughly be delineated for the light phase due to signal overlap; in the heavy fraction these groups are present in notable concentrations.

Both fractions contain significant amounts of aliphatics, as one would principally expect. ^{1}H NMR analyses indicate a significantly higher concentration in aliphatics than in aromatics, which seems to be in contrast to apparent GC results. Yet, it can be assumed that the aliphatics exist mainly in form of fatty acids, which are eventually more difficult to identify in GCMS without derivatization in form of methyl or silyl esters. ^{1}H NMR analyses allows for identifying some biomass-specific differences in the composition of the bio-oils: the pyrolysis of olive stones at 600°C led to the absence of aromatic hydroxyls that corresponds to proximate and ultimate analyses with a low fraction of

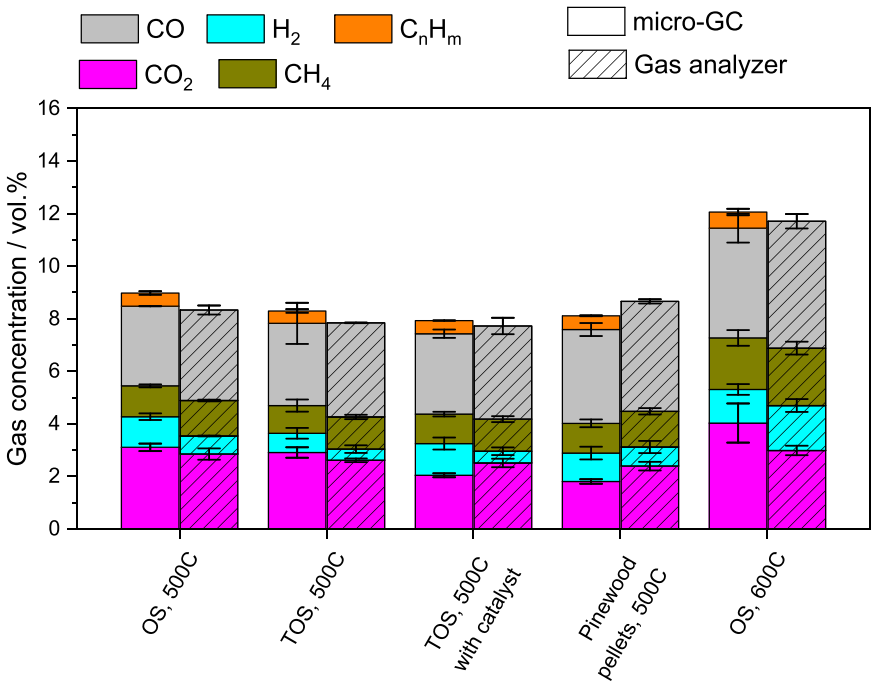

Figure 5. Gas compositional analysis (vol% in inert atmosphere) of the main products from pyrolysis of olive stones, torrefied olive stones, and pinewood pellets at 500 or 600°C with and without catalyst using a micro-GC and a gas analyzer. H_2S gas detected using micro-GC is not shown in this image.

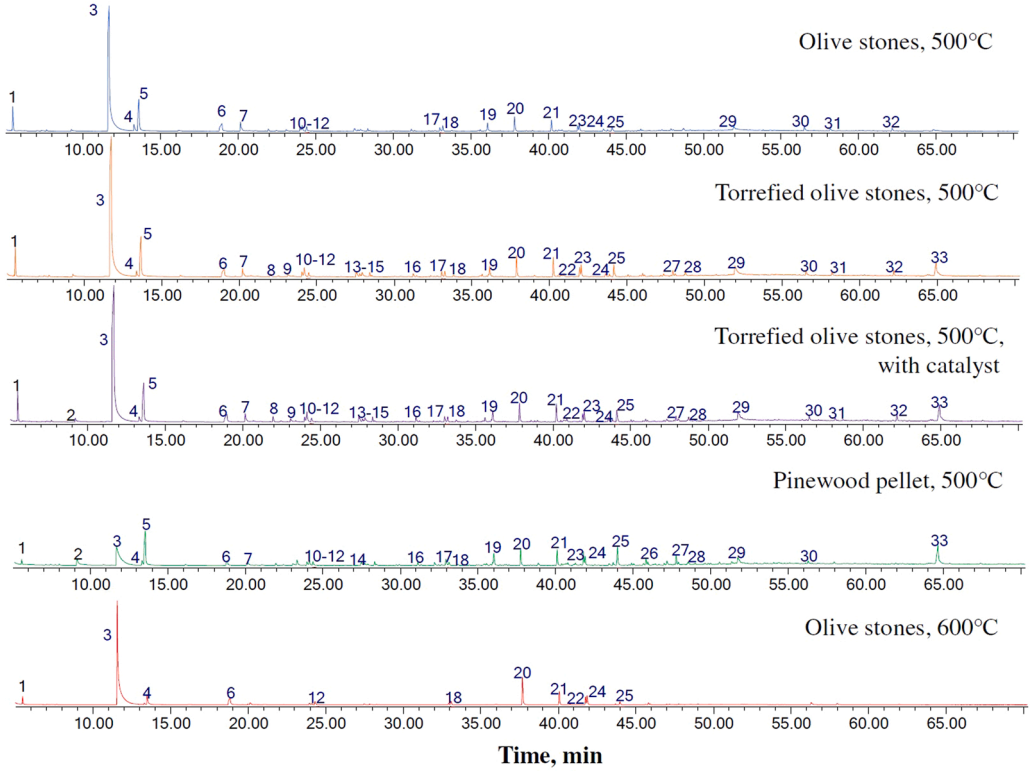

Figure 6. Assignment of peaks from GCMS analysis.

oxygen and water. The release of hydroxyl moieties from aromatic rings can cause the formation of multi-ring compounds through polymerization reactions at 600°C [61].

Figures 7C and B illustrate the ^{1}H NMR spectra of the heavy bio-oil fraction. The composition of bio-oil from pyrolysis of olive stones (**OS**), torrefied material (**TOS**) and catalytically reacted olive stones (**OS**) remained similar. However, observable differences for bio-oil from pyrolysis of pinewood pellets and olive stones at 600°C are mostly present in the aromatic rather than the aliphatic compounds. This corresponds to results of a statistic model that emphasizes the importance of feedstock and temperature on bio-oil yield and composition, also to UV Fluorescence data (see below). Bio-oil from catalytic pyrolysis of olive

Table 3
Compounds identified in the bio-oil sample from pyrolysis of olive stones, torrefied biomass using a catalyst or without and pinewood pellets at 500 or 600°C by GC-MS.

Peak ID	RT, min	Name	Formula	Area, %				
Feedstock				OS	TOS	TOS	PP	OS
Temperature	°C			500	500	500	500	600
Catalyst				no	no	yes	no	no
1	5.49	Acetic acid, methyl ester	$C_3H_6O_2$	3.5	3.1	3.2	1.2	1.9
2	9.19	Acetaldehyde, hydroxy-	$C_2H_4O_2$			0.7	3.4	
3	11.60	Acetic acid	CH_3COOH	61.0	49.9	51.1	23.2	65.6
4	13.28	2-Methoxytetrahydrofuran	$C_5H_{10}O_2$	1.5	0.9	0.8	1.4	3.5
5	13.52	2-Propanone, 1-hydroxy-	$C_3H_7NO_2$	8.8	8.9	8.8	14.6	5.3
6	18.88	Propanoic acid	$C_3H_6O_2$	4.0	3.0	2.8	2.2	
7	20.12	1-Hydroxy-2-butanone	$C_4H_8O_2$	2.4	1.7	1.6	1.5	
8	21.92	Furan, tetrahydro-2,5-dimethoxy-	$C_6H_{12}O_3$		0.4	0.8		
9	23.03	Butanedial	$C_4H_6O_2$		0.5	0.6		
10	23.96	2-Cyclopenten-1-one	C_5H_6O	0.7	0.7	0.7	1.0	
11	24.09	Furfural	$C_5H_4O_2$	1.5	1.7	2.0	1.7	
12	24.35	Butanoic acid	$C_4H_8O_2$	1.2	0.7	0.6	1.2	1.3
13	27.42	2-Propanone, 1-(acetyloxy)-	$C_5H_8O_3$		0.5	0.6	0.8	
14	27.47	2-Cyclopenten-1-one, 2-methyl-	C_6H_8O		0.7	0.6		
15	27.81	1,2-Ethanediol, monoacetate	C_4H_8O		1.0	0.9		
16	31.09	Acetic acid, dimethoxy-, methyl ester	$C_5H_{10}O$		0.5	0.8	0.7	
17	32.94	2-Cyclopenten-1-one, 3-methyl-	C_6H_8O	0.7	0.9	0.8	1.9	
18	33.13	Butyrolactone	$C_4H_6O_2$	1.1	0.8	0.6	0.9	1.4
19	36.01	1,2-Cyclopentanedione, 3-methyl-	$C_3H_8O_2$	1.8	1.6	1.7	3.6	
20	37.74	Phenol	C_6H_6O	3.0	3.0	2.6	4.3	9.5
21	40.11	Phenol, 2-methyl-	C_7H_8O	2.1	2.6	2.4	4.0	4.5
22	40.79	Phenol, 2,6-dimethyl-	$C_8H_{10}O$		0.5	0.4		2.5
23	41.80	Phenol, 4-methyl-	$C_{21}H_{28}O$	0.9	1.2	1.0	3.4	3.3
24	41.90	Phenol, 3-methyl-	$C_{21}H_{28}O$	1.6	1.8	1.5	2.5	
25	44.01	Phenol, 2,3-dimethyl-	$C_8H_{10}O$	1.1	2	1.9	5.2	1.3
26	45.85	Phenol, 4-ethyl-	$C_8H_{10}O$				1.6	
27	47.79	Benzene, 1-ethyl-4-methoxy-	$C_9H_{12}O$		0.7	0.6	2.5	
28	48.62	1,4:3,6-Dianhydro-α-D-glucopyranose	$C_6H_8O_4$		0.7	0.7	1.0	
29	51.79	1,2-Benzenediol	C_6H_6O	0.9	3.6	1.8	3.7	
30	56.32	Resorcinol	$C_6H_6O_2$	1.1	0.9	0.9	1.0	
31	57.98	1,4-Benzenediol, 2-methyl-	C_7H_8O	0.5	0.5	0.5		
32	61.96	Evodone	$C_{10}H_{12}O_2$	0.6	0.9	0.9		
33	64.68	β-D-Glucopyranose, 1,6-anhydro-(levoglucosan)	$C_6H_{10}O$		4.4	5.4	11.1	

stones is characterized by reduction of unsaturated aldehydes which are known as very reactive due to the conjugation of the C-C double group with the carbonyl group [62]. The unsaturated aldehydes, *e.g.*, acrolein could react with alcohol groups in catalytic pyrolysis using zeolites by forming alkoxy aldehydes, unsaturated acetals, or alkoxy acetal compounds or using polymerization path, as reported previously [63,64]. Despite these possibilities, NMR data indicate that neither torrefaction nor the presence of a catalyst change the composition of **OS**-derived bio-oil generated at 500°C. The NMR fingerprint is essentially identical across the species.

3.7. UV fluorescence of bio-oil

Aromatic compounds, such as lignin-based compounds in bio-oil, are known to fluoresce strongly and thus, UV spectra can provide information about the molecular size and the concentration of certain condensed structures [65]. Fig. 8 presents the UV fluorescence spectra acquired of bio-oil samples dissolved in methanol which mainly comprises two absorption bands. A first band near 280 nm corresponds to a $\pi \rightarrow \pi^*$ transition in aromatic compounds, whereas a second one at nearly 325 nm is associated with free etherified hydroxyl groups in bio-oil samples. Compared to conventional fluorescence at fixed wavelength, synchronous fluorescence allows for a much higher spectral resolution for complex mixtures by selecting the appropriate excitation/emission offset according to the molecular structure of the analytes. It was thus possible to separate monomers from oligomers which are potentially more conjugated, and consequently, absorb and emit at longer wavelengths. However, such observation strongly depends on the type of monomer linkage that varies among bio-oil samples.

Figure 8 illustrates the repartition between two types of monomers and oligomers according to a deconvolution of spectra respectively at 306–311, 325 and 370 nm (See supplemental material, Figure S-2).

The first category of monomers is represented by aromatic monomers with hydroxyl and methoxyl groups, *i.e.*, phenol, guaiacol, catechol [66]. Another group includes aromatic monomers with propyl side chains, *i.e.*, iso-eugenol, coniferyl alcohol, sinapyl alcohol, etc. [67]. Oligomers in all bio-oil samples are mostly reported as conjugated aromatics like phenenthrene and anthracene that emit at around 343 nm [68]. The lignin content is greater in pinewood pellets and torrefied olive stones than in olive stones [12] and thus, the monomer content under similar operating conditions (500°C, without catalyst) is greater in bio-oil samples derived from pinewood and torrefied olive stones pyrolysis.

3.8. Rheology

Figure 9 shows the temperature-dependent viscosity of bio-oil samples from pinewood pellets (**PP**), as well as from untreated (**OS**) and torrefied olive stones (**TOS**); viscosities of glycerol and cellulose were measured for comparison. Generally, bio-oil is a Newtonian fluid that does not exhibit hysteresis. Glycerol and bio-oil samples showed qualitatively similar viscosities that varied from 0.5 to 1.8 Pa s which does not change significantly through the entire experiment in the temperature range from 50 to 120°C. The viscosity of cellulose is similar to that of non-Newtonian fluids [69]. The dynamic viscosity of cellulose decreased from 14 to 9 Pa s with increasing temperature from 50 to 90°C. Previous studies have shown that bio-oil viscosity strongly depends on the water content, which ranges from 1.25 to 125 Pa s, at 40°C measurement [57].

The viscosity of bio-oil from fluidized bed pyrolysis was almost 100–200 times lower than that of liquid torrefaction tar and water-wood

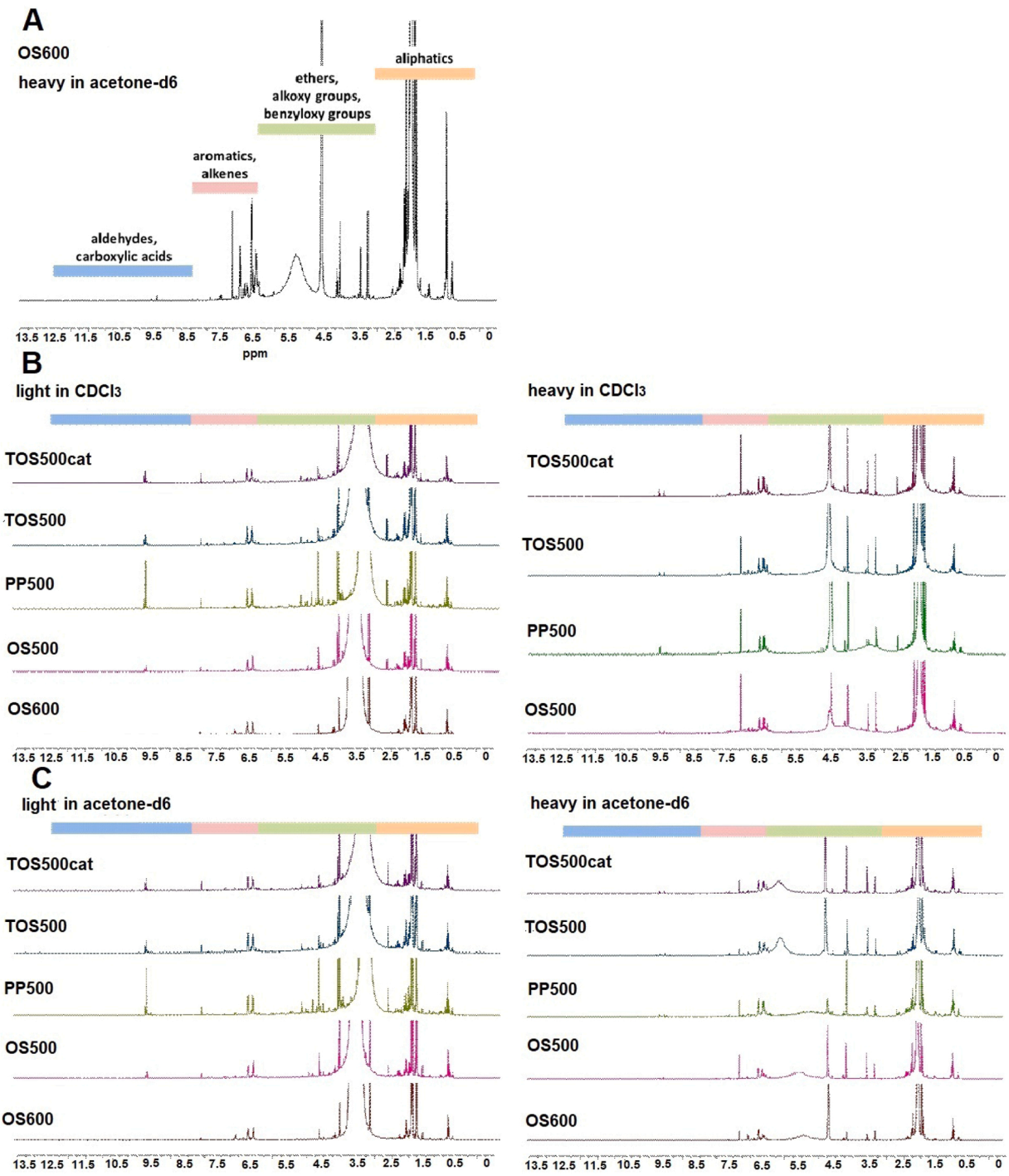

Figure 7. [1]H NMR of bio-oil samples obtained from selected samples: A) exemplary spectra with indication of typical regions for important functional groups; B) comparison of samples divided in light (left) and heavy (right) fractions and analysed in chloroform; C) comparison of samples divided in light (left) and heavy (right) fractions and analysed in acetone-d6.

slurry, reported previously [12,70]. The dynamic viscosity of cellulose decreased from 14 to 9 Pa s with increasing temperature from 50 to 90°C. The viscosity of cellulose is similar to that of non-Newtonian fluids [69]. The viscosity of bio-oil was similar to that of light fossil-based oil (3.5–10 Pa s) [71,72].

4. Discussion

The results of this study show that high yields of bio-oil (30–46 wt%) can be obtained from fluidized bed pyrolysis and further used as a transportation fuel or a value-added chemical after an upgrade. The optimal process parameters for the fluidized bed reactor operation were found using a statistical model for the analysis of product yields and composition which were combined with the optimal parameters suggested in the literature [25,73]. A model emphasized that temperature and feedstock have a more significant impact on the yield and composition of bio-oil from pyrolysis in the fluidized bed reactor. The previous study indicated that torrefaction altered the composition of wood due to reduction of hemicellulose compounds and formation of more lignin-based compounds, leading to low concentrations of light

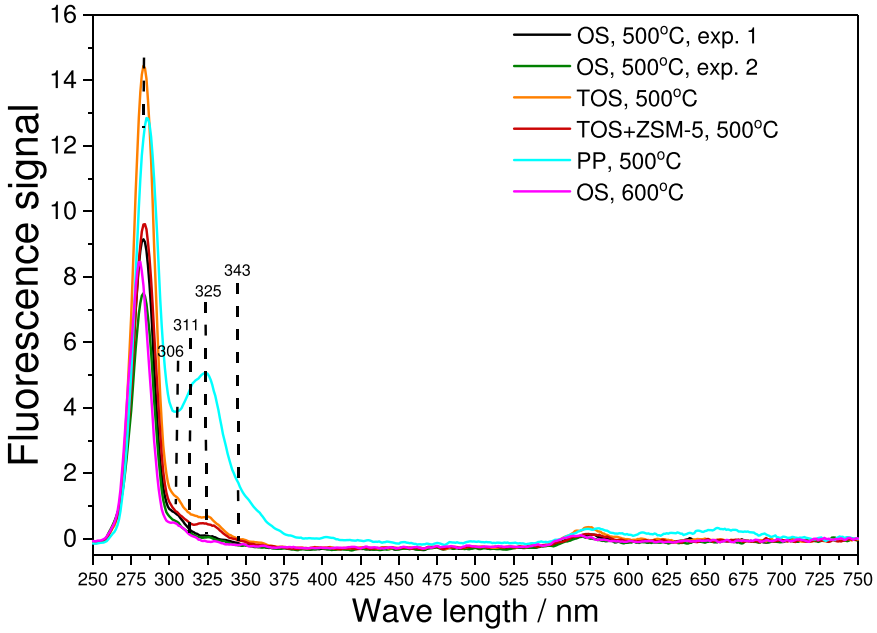

Figure 8. UV Fluorescence analysis of the bio-oil samples.

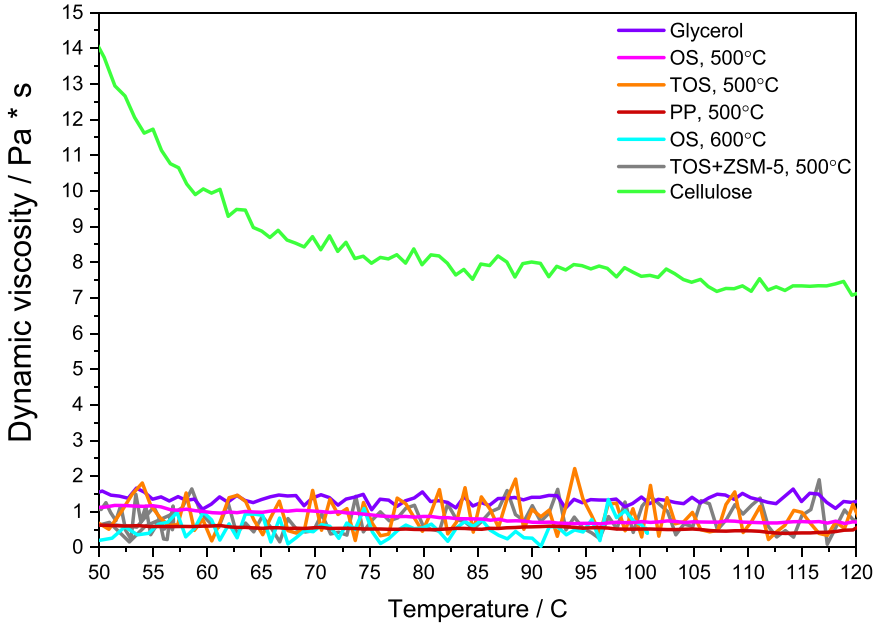

Figure 9. Steady-state flow viscosity of the bio-oil, glycerol, and cellulose.

oxygenates [7]. This could be due to modification of fibers and material composition in torrefaction so that reaction pathways of fluidized bed pyrolysis could be difficult to predict. Chemical analysis of bio-oil from fluidized bed pyrolysis showed that torrefaction temperature affects different types of feedstocks differently due to the variation in hemicellulose, cellulose and lignin fractions, as expected [20]. Olive stones (**OS**) have a higher ash content (0.8 wt%) than pinewood pellets (**PP**) with consequently higher concentrations of Ca, K, and Si (see Table 1) [26]. However, **OS** contain less cellulose and more hemicellulose than **PP**, whereas the amount of lignin is similar in both feedstocks [27]. The different composition of hemicelluloses in olive stones and pinewood pellets could also affect the results [74]. The high amount of alkali metals and low fraction of cellulose in the untreated **OS** could lead to a small mass loss of torrefied material during fast fluidized pyrolysis. In opposite to results from the previous study, use of torrefied wood as a feedstock led to a significant mass loss in fluidized bed pyrolysis [19].

Another observation in this study is related to low impact of the catalyst on the yield and composition of bio-oil. Despite the fact of fewer unsaturated aldehydes in the catalytic pyrolysis of olive stones, the composition and rheological properties were similar to other bio-oil samples. All bio-oil samples contained mostly monomers and oligomers without any presence of polymers, as UV fluorescence analysis reported. This study underlined the importance of combined analytical analysis of bio-oil properties. Combined GCMS and ^{1}H NMR were capable to detect aliphatic and aromatic alcohol, aldehydes, alkyl aryl ethers, unsaturated compounds, aromatic amines, diols, and acids. The pinewood pellet bio-oil contained a higher fraction of aromatic alcohols. The impact of temperature on bio-oil composition was observed in

stronger polymerization reaction during pyrolysis of olive stones at 600°C. Table 4 shows the comparison of physical properties of bio-oil samples and fossil-based heavy fuel oil and light motor oil.

Overall, the bio-oil samples from fluidized bed pyrolysis in the present research seem to be in a good agreement with the required properties for a successful downstream processing at aviation and power plant [57,63,77,78]. In comparison to other fuel oils, the high oxygen content of bio-oil is the primary reason for differences in its properties and behaviour. This results in immiscibility with hydrocarbon fuels and a very low energy density both on a wet and dry basis. The results of this work showed that bio-oil from pyrolysis of olive stones (**OS**) at 600°C has the lowest oxygen and water content of 14.4 wt% and 10.4 wt% respectively. This also highlights the importance of reaction temperature on the bio-oil composition. In addition, this work determined low amounts of organically bound nitrogen in bio-oil that varied from 0.3 to 1.7 wt%, as shown in Table 2. The low concentrations (0.02 wt%) of organically bound sulphur in untreated olive stones (**OS**) remained at the same level in the torrefied material, *i.e.*, **TOS**, as shown in Table 1.

The novelty of this work relies on the fact that product yields and properties of bio-oil from fluidized bed pyrolysis seems to strongly depend on the feedstock type and reaction temperature. The present statistical model is a first step to predict and evaluate the properties of pyrolysis bio-oil that can be further extended to a maturity model for the assessment of effectiveness of current experimental design as well as for the development of a roadmap to improve the bio-oil quality. More research will be required regarding the use of torrefied feedstocks in fluidized bed pyrolysis aiming to produce fuels and value-added chemicals on an industrial scale.

5. Conclusion

This work demonstrates that feedstock type and reaction temperature have a stronger impact on the product yields and composition than torrefaction pre-treatment of biomass before fluidized bed pyrolysis. The integration of torrefied feedstocks into pyrolysis process strongly depends on the lignocellulosic composition and properties of original biomass. Addition of ZSM-5 catalyst increased the yields of levoglucosan. The composition of bio-oil from fast pyrolysis was pre-dominated by phenols, BTX, oxygenated aliphatics. This creates potential for the further development of a mechanism to tune bio-oil properties towards aliphatic or aromatic composition with respect to application field. Pyrolysis of olive stones at 600°C showed the most homogeneous composition of bio-oil with the lowest content of oxygen and water and pyrolysis of pinewood provided bio-oil with a more aromatic composition than aliphatic. The presence of organically bound sulphur and nitrogen was below commercial fuel use limits, making it more promising as either a direct liquid fuel or as a fossil oil blend, for application in aviation or power plant industries.

CRediT authorship contribution statement

Anna Trubetskaya: Conceptualization, Methodology, Software, Investigation, Data curation, Visualization, Writing – original draft, Writing – review & editing. **Lukas von Berg:** Conceptualization, Validation, Formal analysis, Investigation, Writing – review & editing. **Robert Johnson:** Validation. **Sean Moore:** Software, Validation, Investigation, Data curation. **JJ Leahy:** Formal analysis, Investigation, Resources, Supervision, Project administration. **Yinglei Han:** Conceptualization, Formal analysis, Writing – review & editing, Funding acquisition. **Heiko Lange:** Formal analysis, Investigation, Resources, Data curation, Writing – review & editing. **Andres Anca-Couce:** Conceptualization, Methodology, Investigation, Resources, Writing – review & editing, Supervision, Funding acquisition.

All authors have read and agreed to the published version of the manuscript.

Table 4
Physical properties of fossil-based aviation fuels (heavy duty oil and light motor oil) and bio-oil (previous study at VTT and current project).

	Heavy duty oil [73]	Light motor oil [57]	Bio-oil [57]	OS Bio-oil current study
S, (wt% db)	below 1	max. 0.001	below 0.05	below 0.002
N, (wt% db)	below 0.4	below 0.02	0.4–4.6 ([57, 75])	0.3–1.7
Water, (wt% ar)	≈ 0	≈ 0	20–30	9–20
Ash, (wt% db)	below 0.5	below 0.5	0.01–0.1	0.02–0.06
Viscosity, (at 40°C)	5–15 ([76])	3.5–10 ([71, 72])	1.25–125 ([57])	0.5–1.8
pH			2–3	1.8–2.5
Stability			Unstable	Unstable
Solids	max. 0.5	max. 0.02	below 0.5	below 0.2

Declaration of Competing Interest

The authors declare that they have no known competing financial interests or personal relationships that could have appeared to influence the work reported in this paper.

Data Availability

No data was used for the research described in the article.

Acknowledgements

The authors gratefully acknowledge financial support from Science Foundation Ireland (Grant number 16/SP/3829) and Arigna Fuels under the Sustainable Energy and Fuel Efficiency (SEFE) spoke of the Research Centre for Marine and Renewable Energy (MaREI). The authors gratefully acknowledge financial support (Grant number 731101) given by European Union's Horizon 2020 Research and Innovation Programme (BRISK II). Dr. Gerrit Ralf Surup from NTNU is acknowledged for technical support on Karl Fisher titration and elemental analysis.

Appendix A. Supporting information

Supplementary data associated with this article can be found in the online version at doi:10.1016/j.jaap.2022.105841.

References

[1] European Commission, Communications from the Commission to the European Parliament, the European Council, The Council, The European Economic and Social Committee and the Committee of the Regions, Eur. Green Deal Rep. 640 (2019) 24.
[2] Y. Kalmykova, M. Sadagopan, L. Rosado, Circular economy - from review of theories and practices to development of implementation tools, Resour. Conserv. Recycl. 135 (2018) 190–201.
[3] F. Scala, R. Chirone, P. Salatino, Combustion and attrition of biomass chars in a fluidized bed, Energy Fuels 20 (2006) 91–102.
[4] M. Zenvenhoven-Onderwater, R. Backman, B.J. Skrifvars, M. Hupa, T. Liliendahl, K. Engvall, et al., The ash chemistry in fluisied bed gasification of biomass fuels. Part II: Ash behaviour prediction versus bench scale agglomeration tests, Fuel 80 (2001) 1503–1512.
[5] A.V. Bridgwater, Renewable fuels and chemicals by thermal processing of biomass, Chem. Eng. J. 91 (2003) 87–102.
[6] A. Aho, N. Kumar, T. Salmi, M. Hupa, D.Y. Murzin, K. Eränen, Catalytic pyrolysis of biomass in a fluidized bed reactor: Influence of the Acidity of H-Beta Zeolite, Trans. Int. Chem. Eng. Part B 85 (2007) 473–480.
[7] J. Meng, J. Park, D. Tilotta, S. Park, The effect of torrefaction on the chemistry of fast-pyrolysis bio-oil, Bioresour. Technol. 111 (2012) 439–446.
[8] C. Villemont, O. Rezazgui, B. Delcroix, S. Barnabe, D. Montplaisir, P. Mangin, Testing a novel, mechanically fluidized bed pilot unit intended for the production of bio-oil and biochar from forest biomass, Ind. Biotech. 15 (2019) 179–187.
[9] S. Ren, H. Lei, L. Wang, Q. Bu, S. Chen, J. Julson, et al., The effects of torrefaction on compositions of bio-oil and syngas from biomass pyrolysis by microwave heating, Bioresour. Technol. 135 (2013) 659–664.

[10] M. Atienza-Martinez, I. Rubio, I. Fonts, G. Gea, Effect of torrefaction on the catalytic post-treatment of sewage sludge pyrolysis vapors using γ-Al_2O_3, Chem. Eng. J. 308 (2017) 264–274.

[11] M. Atienza-Martinez, I. Fonts, J. Ceamanos, G. Gea, Effects of temperature and holding time during torrefaction on the pyrolysis behaviors of woody biomass, Chem. Eng. J. 259 (2015) 467–480.

[12] A. Trubetskaya, R. Johnson, R.F.D. Monaghan, A.S. Ramos, A. Brunsvik, V. Budarin, et al., Combined analytical strategies for chemical and physical characterization of tar from torrefaction of olive stone, Fuel 291 (2021), 120086.

[13] J. Wannapeera, B. Fungtammasan, N. Worasuwannarak, Effects of temperature and holding time during torrefaction on the pyrolysis behaviors of woody biomass, J. Anal. Appl. Pyrolysis 92 (2011) 99–105.

[14] T. Wigley, A.C.K. Yip, S. Pang, Pretreating biomass via demineralisation and torrefaction to improve the quality of crude pyrolysis oil, Energy 109 (2016) 481–494.

[15] A.A. Boateng, C.A. Mullen, Fast pyrolysis of biomass thermally pretreated by torrefaction, J. Anal. Appl. Pyrolysis 100 (2013) 95–102.

[16] H.V. Ly, B. Kwon, J. Kim, C. Oh, H.T. Hwang, Lee J. Suk, et al., Effects of torrefaction on product distribution and quality of bio-oil food waste pyrolysis in N_2 and CO_2, Waste Manag. 141 (2022) 16–26.

[17] A.N. Gayubo, A.T. Aguayo, A. Atutxa, R. Prieto, J. Bilbao, Deactivation of a HZSM-5 zeolite catalyst in the transformation of the aqueous fraction of biomass pyrolysis oil into hydrocarbons, Energy Fuels 18 (2004) 1640–1647.

[18] S. Neupane, S. Adhikari, Z. Wang, A.J. Ragauskas, Y. Pu, Effect of torrefaction on biomass structure and hydrocarbon production from fast pyrolysis, Green Chem. 17 (2015) 2406–2417.

[19] H. Li, X. Liu, S. Sokhansanj, J.C. Lim, X.T. Bi, Torrefaction of sawdust in a fluidized bed reactor, Bioresour. Technol. 103 (2011) 453–458.

[20] G.A. Tsalidis, C. Tsekos, K. Anastasakis, W. de Jong, The impact of dry torrefaction on the fast pyrolysis behavior of ash wood and commercial Dutch mixed wood in a pyroprobe, Fuel Process. Technol. 177 (2018) 255–265.

[21] E.T. Ganda, P. Branchi, M. Urciuolo, R. Migliaccio, A. Coppola, F. Scala, et al., Catalytic pyrolysis of torrefied olive stone for production of potential petrochemical alternatives, Biofuels Bioprod. Biorefin. (2022) 1–10.

[22] T. Yoshikawa, S. Shinohara, T. Yagi, N. Ryumon, Y. Nakasaka, T. Tago, et al., Production of phenols from lignin-derived slurry liquid using iron oxide catalyst, Appl. Catal. B Environ. 146 (2014) 289–297.

[23] J. Zakzeski, P.C.A. Bruijnincx, A.L. Jongerius, B.M. Weckhuysen, The catalytic valorization of lignin for he production of renewable chemicals, Chem. Rev. 110 (2010) 3552–3599.

[24] A.L. Mayedo, Comparing Optical and High-Resolution Mass Spectrometry Methods to Characterize the Chemical Composition of Terrstrially-Sourced Dissolved Organic Carbon, Elsevier, 2018.

[25] L. von Berg, G. Pongratz, A. Pilatov, H. Almuina-Villar, C. Hochenauer, R. Scharler, et al., Correlations between tar content and permanent gases as well as reactor temperature in a lab-scale fluidized bed biomass gasifier applying different feedstock and operating conditions, Fuel 305 (2021), 121531.

[26] A. Trubetskaya, J.J. Leahy, R. Johnson, J. Grams, RFD G.Monaghan, The effect of particle size, temperature and residence time on the yields and reactivity of olive stones from torrefaction, Renew. Energy 160 (2020) 998–1011.

[27] A. Trubetskaya, J.J. Leahy, E. Yazhenskikh, P. Layden, R. Johnson, R.F. D. Monaghan, et al., Characterization of woodstove briquettes from torrefied biomass and coal, Energy 171 (2019) 853–865.

[28] P. Sangines, M.P. Dominguez, F. Sanchez, G. San Miguel, Slow pyrolysis of olive stones in a rotary kiln: chemical and energy characterization of solid, gas, and condensable products, J. Renew. Sustain. Energy 7 (2015) 1–13.

[29] N. Koukouzas, D. Papanikolaou, A. Tourunen, T. Jäntti, J. Hämäläinen, High heating rate devolatilization kinetics of pulverized biomass fuels, Energy Fuels 32 (2018) 12955–12961.

[30] Trubetskaya, A. Biomass fast pyrolysis at high temperatures. PhD thesis, Technical University of Denmark, 2015. https://orbit.dtu.dk/en/publications/fast-pyrolysis-of-biomass-at-high-temperatures.

[31] F.J. Frandsen. Deposition and Corrosion When Utilizing Straw for Heat and Power Production. Doctoral thesis, Technical University of Denmark, 2010.

[32] F. Melligan, M.H.B. Hayes, W. Kwapinski, J.J. Leahy, Hydro-pyrolysis of biomass and online catalytic vapor upgrading with Ni-ZSM-5 and Ni-MCM-41, Energy Fuel 26 (2012) 6080–6090.

[33] R. Liu, C. Deng, J. Wang, Fast pyrolysis of corn straw for bio-oil production in a bench-scale fluidized bed reactor, Energy Sources Part A 32 (2010) 10–19.

[34] A. Trubetskaya, P.A. Jensen, A.D. Jensen, M. Steibel, H. Spliethoff, P. Glarborg, et al., Comparison of high temperature chars of wheat straw and rice husk with respect to chemistry, morphology and reactivity, Biomass Bioenergy 86 (2016) 76–87.

[35] A. Trubetskaya, Reactivity effects of inorganic content in biomass gasification: a review, Energies 15 (2022) 1–36.

[36] M. Thommes, Physical adsorption characterization of nanoporous materials, Chem. Ing. Tech. 82 (2010) 1059–1073.

[37] Z. Wang, Q. Guo, X. Liu, C. Cao, Low temperature pyrolysis characteristics of oil sludge under various heating conditions, Energy Fuel 21 (2007) 957–962.

[38] X. Wang, S.R.A. Kersten, W. Prins, W.P.M. van Swaaij, Biomass pyrolysis in a fluidized bed reactor. Part 2: experimental validation of model results, Ind. Eng. Chem. Res 44 (2005) 8786–8795.

[39] B. Zhang, S. Xiong, B. Xiao, D. Yu, X. Jia, Mechanism of wet sewage sludge pyrolysis in a tubular furnace, Int J. Hydrog. Energy 36 (2011) 355–363.

[40] X. Hu, M. Gholizadeh, Biomass pyrolysis: a review of the process development and challenges from initial researches up to the commercialisation stage, J. Energy Chem. 39 (2019) 109–143.

[41] Y. Liu, C. Ran, A.R. Siddiqui, X. Mao, Q. Kang, J. Fu, et al., Pyrolysis of textile dyeing sludge in fluidized bed: characterization and analysis of pyrlysis products, Energy 165 (2018) 720–730.

[42] P.O. Morf, Secondary Reactions of Tar during Thermochemical Biomass Conversion. PhD thesis ETH Zurich, 2001.

[43] T. Li, K. Miao, Z. Zhao, Y. Li, H. Wang, A. Watanabe, et al., Understanding cellulose pyrolysis under hydrogen atmosphere, Energy Convers. Manag. (2022), 115195.

[44] I. Muhammad, G. Manos, Improving the conversion of biomass in catalytic pyrolysis via intensification of biomass - catalyst contact by co-pressing, Catalysts 11 (2021) 1–20.

[45] J. Piskorz, D.S.A.G. Radlein, D.S. Scott, S. Czernik, Pretreatment of wood and cellulose for production of sugars by fast pyrolysis, J. Anal. Appl. Pyrolysis 16 (1989) 127–142.

[46] N. Ali, M. Saleem, K. Shahzad, S. Hussain, A. Chughtai, Effect of operating parameters on production of bio-oil from fast pyrolysis of maize stalk in bubbling fluidized bed reactor, Pol. J. Chem. Tech. 18 (2016) 88–96.

[47] J.E. Omoriyenkomwan, A. Tahmasebi, J. Yu, Production of pehnol-rich bio-oil during catalytic fixed-bed and microwave pyrolysis of palm kernel shell, Bioresour. Technol. 207 (2016) 188–196.

[48] P. Alizadeh, L.G. Tabil, P.K. Adapa, D. Cree, E. Mupondwa, B. Emadi, Torrefaction and densification of wood sawdust for bioenergy applications, Fuels 3 (2021) 152–175.

[49] E. Barta-Rajnai, Z. Sebestyen, E. Jakab, E. Patus, J. Bozi, L. Wang, et al., Pyrolysis of untreated and various torrefied stem wood, and bark of Norway spruce, Energy Fuels 33 (2019) 3210–3220.

[50] G. Lyu, S. Wu, H. Zhang, Estimation and comparison of biooil components from different pyrolysis conditions, Front. Energy Res. 3 (2015), 1-1.

[51] C.S. Badal, Hemicellulose bioconversion, J. Ind. Microbiol. Biotechnol. 30 (2003) 279–291.

[52] P.M.A. Pawar, S. Koutaniemu, M. Tenkanen, E.J. Mellerowicz, Acetylation of woody lignocellulose: significance and regulation, Front. Plant Sci. 4 (2013) 1–8.

[53] G. Pongratz, V. Subotic, L. von Berg, H. Scroettner, G. Hochenauer, S. Martini, et al., Real coupling of solid oxide fuel cells with a biomass steam gasifier: operating boundaries considering performance, tar and carbon deposition analyses, Fuel 316 (2022), 123310.

[54] M. Siriwardhana. Aging and Stabilization of Pyrolytic Bio-oils and Model Compounds. MSc thesis, The University of Western Ontario, 2013.

[55] S. Omar, S. Alsamag, Y. Yang, J. Wang, Production of renewable fuels by blending bio-oil with alcohols and upgrading under supercritical conditions, Front. Chem. Sci. Eng. 13 (2019) 702–717.

[56] M.E. Boucher, A. Chaala, C. Roy, Bio-oils obtained by vacuum pyrolysis softwood bark as a liquid fuel for gas turbine. Part I: Properties of bio-oil and its blends with methanol and a pyrolytic aqueous phase, Biomass & Bioenergy 19 (2000) 337–350.

[57] J. Lehto, A. Oasmaa, Y. Solantausta, M. Kytö, D. Chiaramonti, Fuel oil quality and combustion of fast pyrolysis biooil, VTT Technol. 87 (2013) 1–79.

[58] L. Devi, K.J. Ptasinski, F.J.J.G. Janssen, S.V.B. van Paasen, P.C.A. Bergman, J.H. A. Kiel, Catalytic decomposition of biomass tars: use of dolomite and untreated olivine, Renew. Energy 30 (2005) 565–587.

[59] Y. Kostyukevich, M. Vlaskin, A. Zherebker, A. Grigorenko, L. Borisova, E. Nikolaev, High-resolution mass specrometry study of the bio-oil samples produced by thermal liquefaction of microalgae in different solvents, J. Am. Soc. Mass Spectrom. 30 (2019) 605–614.

[60] N. Hao, H. Ben, C.G. Yoo, S. Adhikari, A.J. Ragauskas, Review of NMR characterization of pyrolysis oils, Energy Fuels 30 (2016) 6863–6880.

[61] M.S. Safdari, E. Amini, D.R. Weise, T.H. Fletcher, Heating rate and temperature effects on pyrolysis products from live wildland fuels, Fuel 242 (2019) 295–304.

[62] W.G. Etzkorn, J.J. Kurland, W.D. Neilsen, Acrolein and Derivatives in Kirk and Otheras Encyclopedia of Chemical Technology, volume 1, John Wiley and Sons, 1991.

[63] J. Diebold, A Review of the Chemical and Physical Mechanisms of the Storage Stability of Fast Pyrolysis Bio-Oils, NREL Report / SR-570–27613 (2000)1–59.

[64] Y. Han, M. Gholizadeh, C.C. Tran, S. Kaliaguine, C.Z. Li, M. Olarte, et al., Hydrotreatment of pyrolysis bio-oil: A review, Fuel Process. Technol. (2019), 106140.

[65] F. Stankovikj, A.G. McDonald, G.L. Helms, M. Garcia-Perez, Quantification of bio-oil functional groups and evidences of the presence of pyrolytic humins, Energy Fuels 30 (2016) 6505–6524.

[66] E. Bartolomei, Y. LeBrech, A. Dufour, V. Carre, F. Aubriet, E. Terrell, et al., Lignin depolymerization: comparison of methods to analyze monomers and oligomers, ChemSusChem 13 (2020) 4633–4648.

[67] C.P. Rodrigo, W.H. James, T.S. Zwier, Single-conformation ultraviolet and infrared spectra of jet-cooled monolignols: p-coumaryl alcohol, coniferyl alcohol, and sinapyl alcohol, J. Am. Chem. Soc. 133 (2011) 2632–2641.

[68] E. Pines, Chapter 7: UV-Visible spectra and photoacidity of phenols, naphtols and pyrenols, ChemInform 36 (2005) 491–527.

[69] F. Conti, L. Wiedemann, M. Sonnleitner, M. Goldbrunner, Thermal behaviour of viscosity of aqueous cellulose solutions to emulate biomass in anaerobic digesters, New J. Chem. 42 (2018) 1099–1104.

[70] W. He, C.S. Park, J.M. Norbeck, Rheological study of comingled biomass and coal slurries with hydrothermal pretreatment, Energy Fuels 23 (2009) 4763–4767.

[71] K. Sirviö, S. Niemi, R. Help, S. Heikkilä, E. Hiltunen, Kinematic viscosity studies for medium-speed CI engine fuel blends, Agron. Res. 16 (2018) 1247–1256.

[72] H. Bennadji, L. Khachatryan, M. Lomnicki, Kinematic modeling of cellulose fractional pyrolysis, Energy Fuels 32 (2018) 3436–3446.
[73] A. Oasmaa, C. Peacocke. Properties and fuel use of biomass-derived fast pyrolysis liquids: A guide, VTT Technical Research Centre of Finland, 2010.
[74] D. Magalhaes, L. Matsakas, P. Christakopoulos, I. Pisano, J.J. Leahy, F. Kazanc, et al., Prediction of yields and composition of char from fast pyrolysis of commercial lignocellulosic materials, organosolv fractionated and torrefied olive stones, Fuel 289 (2021), 119862.
[75] C.A. Mullen, A. Boateng, J. Wang, Chemical composition of bio-oils produced by fast pyrolysis of two energy crops, Energy Fuels 22 (2008) 2104–2109.
[76] T. Sencic, V. Mrzljak, B. Bonefacic, 2D CFD simulation of water injection strategies in a large marine engine, J. Mar. Sci. Eng. 7 (2019) 1–18.
[77] S. Cheng, L. Wei, X. Zhao, J. Julson, Application, deactivation, and regeneration of heterogeneous catslysts in bio-oil upgrading, Catalysts 6 (2016) 1–24.
[78] A. Oasmaa, D.C. Elliott, S. Müller, Quality control in fast pyrolysis bio-oil and use, Environ. Prog. Sustain Energy 28 (2009) 404–409.